# Effect of Neodymium Substitution on Structural, Magnetic and Electrical Properties of Cobalt Ferrite Nanoparticles

*Milind (Physics), Researcher, Sunrise University, Alwar (Raj.)*
*Dr. Vipin Kumar (Physics), Professor, Sunrise University, Alwar (Raj.)*

## Abstract

*This study explores the influence of neodymium ($Nd^{3+}$) doping on the structural, magnetic, and electrical properties of cobalt ferrite ($CoFe_{2-x}Nd_xO_4$) nanoparticles synthesized via the sol-gel method. XRD and TEM analyses confirmed the formation of a single-phase spinel structure with a concentration-dependent growth in crystallite size. Neodymium doping resulted in a decrease in saturation magnetization, attributed to the substitution of $Fe^{3+}$ ions with $Nd^{3+}$ ions at the octahedral sites. Coercivity was found to be particle size dependent. Electrical resistivity and dielectric properties were also affected, with the latter demonstrating a frequency and temperature dependence, explained through Maxwell-Wagner interfacial polarization and electron hopping mechanisms. The findings illustrate the potential of neodymium doping in tuning the magnetic and electrical properties of cobalt ferrite nanoparticles for diverse technological applications.*

*Keywords: Crystallite Size, Coercivity, Neodymium, Sol-gel Method*

## INTRODUCTION

An important group of chemicals, spinel ferrites exhibit a wide range of magnetic, electrical, and catalytic properties [1-3]. Cobalt ferrite stands out among the other ferrite materials for its exceptional coercivity, modest saturation magnetization, great chemical stability, and high mechanical toughness. There are several technological uses for cobalt ferrite, such as in high density recording media, magnetic fluids, magnetic refrigerants, and targeted medication delivery [4, 5]. The size and size distribution of ferrite nanoparticles, which are directly related to the process of synthesis, have a significant impact on their magnetic and electrical properties [6]. The manufacturing of cobalt ferrite nanoparticles with the desired size and characteristics remains difficult despite the introduction of many synthesis techniques. The manufacture of ferrite nanoparticles can be done using a variety of popular chemical and physical approaches. The sol-gel approach is an advantageous method because it allows for precise regulation of stoichiometry, crystallite size, and particle distribution [7].

The effect of doping with various rare earth ions on the characteristics of ferrites has been studied by a number of researchers. According to these analyses, changing the composition of the material by replacing a small fraction of the $Fe^{3+}$ ions with rare earth ions causes strain and structural distortion, hence altering the material's magnetic and electrical properties [8-10]. Substitution of $Fe^{3+}$ with $Pr^{3+}$ and $Gd^{3+}$ in $CoFe_2O_4$ produced using the citrate precursor approach has been shown by Panda et al. [11] to significantly modify the magnetic characteristics and decrease the grain size of the material. The magnetic characteristics of samarium-substituted $CoFe_2O_4$ produced via the citrate precursor technique were investigated by Rashad et al. [12]. The impact of $La^{3+}$ doping on the electric, dielectric, and magnetic characteristics of cobalt ferrite via the co-precipitation method has been studied by Pawan et al. . The potential uses of cobalt based ferrite nanoparticles in high density information storage and tailored transport of pharmaceuticals have piqued the interest of scientists in recent years. However, we must be able to tune the magnetic characteristics of these materials in order to meet the requirements of these applications. It is possible to manipulate ferrite's magnetic characteristics by changing its chemical composition by introducing divalent or trivalent cations. Due to the large fluctuation in the quantity of 4f electrons, rare earth ions are said to exhibit a wide range of magnetic characteristics. Doping cobalt ferrite with neodymium ions will be an attractive option for changing the material's magnetic characteristics. Cobalt ferrite nanoparticles made via the sol gel method have yet to be studied for how neodymium

substitution affects their characteristics. In this work, we use the sol-gel method to synthesize cobalt ferrite ($CoFe_{2-x}NdxO_4$ with x=0.0 to 0.25 in steps of 0.05) and examine how the addition of neodymium affects its structural and magnetic properties.

## SYNTHESIS

Nanoparticles of neodymium doped cobalt ferrite ($CoFe_{2-x}NdxO_4$) were produced using the sol-gel method (with x=0.0 to 0.25 in steps of 0.05). A magnetic stirrer was used to dissolve cobalt nitrate, neodymium nitrate, and ferric nitrate (AR grade MERCK) in the smallest amount of ethylene glycol possible. To obtain a wet gel of the metal nitrate, the solution was heated to 333K. The gel was dried at high temperatures, which caused it to self-ignite, resulting in a very light and airy final product. Ethylene glycol serves as the reducing agent and nitrate ion serves as the oxidant in this combustion, which may be thought of as a redox reaction of the gel triggered by heat. The resulting powder was finely milled before being sintered for 4 hours at 673K in a muffle furnace.

## FINDINGS AND INTERPRETATION

### Analysis by X-Ray Diffraction

Figure 1 displays the XRD patterns of $CoFe_{2-x}NdxO_4$ nanoparticles sintered at 673K (with x=0.0 to 0.25 in steps of 0.05). By comparing each sample's XRD pattern to reference data (JCPDS PDF Card No. 22-1086), we were able to confirm that spinel structure had formed in every one. All of the samples show a minuscule amount of hematite phase (- $Fe_2O_3$), and the peak corresponding to this phase becomes noticeable at x=0.25. An impurity phase known as hematite commonly forms in ferrites.
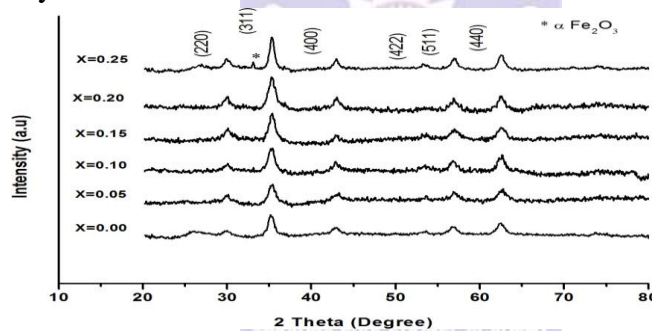


**Figure 1: XRD patterns of $CoFe_{2-x}NdxO_4$ system**

For a prominent peak (311), the lattice parameter 'a' is derived by solving for the interplanar spacing dhkl using Bragg's equation. The bulk cobalt ferrite lattice parameter determined from an undoped sample agrees well with previous estimates . As the neodymium level of the cobalt ferrite samples is raised, so are the lattice parameters. $Nd^{3+}$ has a larger ionic radius than $Fe^{3+}$ (0.0645nm vs. 0.0983nm). Neodymium ions added to a ferrite lattice cause the unit cell to enlarge, which in turn raises the lattice parameter. There have been reports of similar findings .The average crystallite size was determined by plotting all of the samples on a Hall-Williamson diagram .Our prior work [8] provides the specifics of the Hall-Williamson study. As neodymium content rises, so does the average size of the crystallites. Table 1 displays the obtained lattice parameter and average crystallite size for all samples. Samples with lower amounts of neodymium show a smaller rise in crystallite size. For x=0.25, however, there is a notable improvement. Researchers have found that as rare earth concentration rises, so does the grain size of ferrite samples. Increases in grain size, as seen, are indicative of high chemical homogeneity of the produced samples, as stated by Binu et al. [7] and Tahar et al.  This, according to Jianhong et al. ,was caused by the presence of unaccounted-for phases in the samples. There are no supplementary peaks in the XRD pattern here that would be attributable to neodymium oxides. However, a secondary phase of iron oxide (-$Fe_2O_3$) may account for the dramatic growth in crystallite size at x=0.25.

**Table 1: Effect of Nd$^{3+}$ doping on the lattice parameter, crystallite size, density, porosity and particle size of CoFe$_{2-x}$NdxO$_4$**

| Nd content X | Lattice parameter(A) | Crystalline size(nm) | X-ray density(g cm-3) | Bulk density(g cm-3) | Porosity (%) | Particle size(nm) |
|---|---|---|---|---|---|---|
| 0.00 | 8.399 | 11.26 | 5.260 | 2.662 | 48.96 | 15.3 |
| 0.05 | 8.422 | 13.00 | 5.315 | 2.716 | 48.27 | |
| 0.10 | 8.424 | 13.38 | 5.408 | 2.690 | 50.23 | 18.3 |
| 0.15 | 8.425 | 14.04 | 5.504 | 2.581 | 53.12 | |
| 0.20 | 8.428 | 14.69 | 5.598 | 2.461 | 56.02 | |
| 0.25 | 8.432 | 17.64 | 5.689 | 2.665 | 53.14 | 23.3 |

**Transmission Electron Microscopy Analysis:** TEM images of CoFe$_{2-x}$NdxO$_4$ samples at x=0.0, 0.1, and 0.25 are shown in Figures 2(a)-(c). Most of the nanoparticles have a roundish form, while some are lumped together. Figures 3(a)-(c) depict the size distribution of the nanoparticles as seen in TEM images. The size distribution of the samples is rather tight. Table 1 displays the average particle sizes as determined by TEM examination, as depicted in Figures 3(a)–(c). The size distribution of the samples is rather tight. Table 1 displays the average particle sizes as determined by TEM examination.
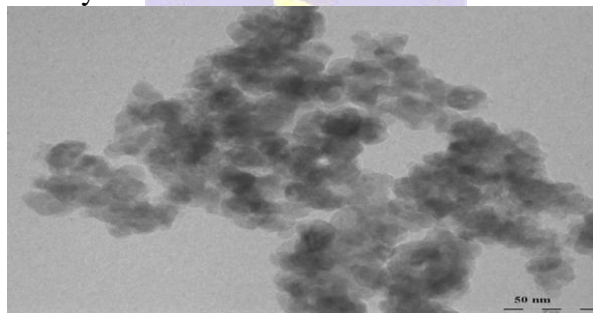


**Figure 2(a) TEM image of CoFe$_2$O$_4$**
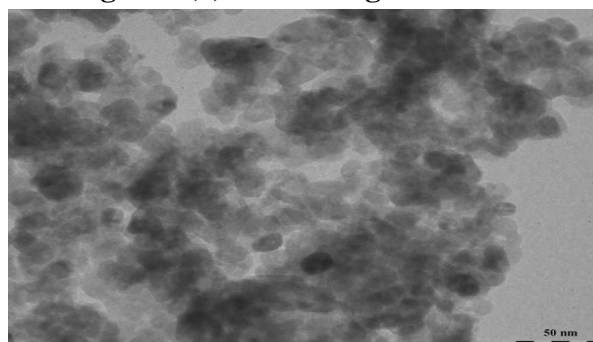


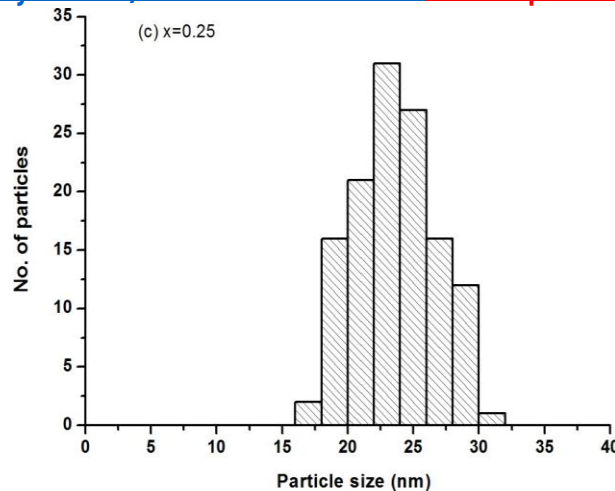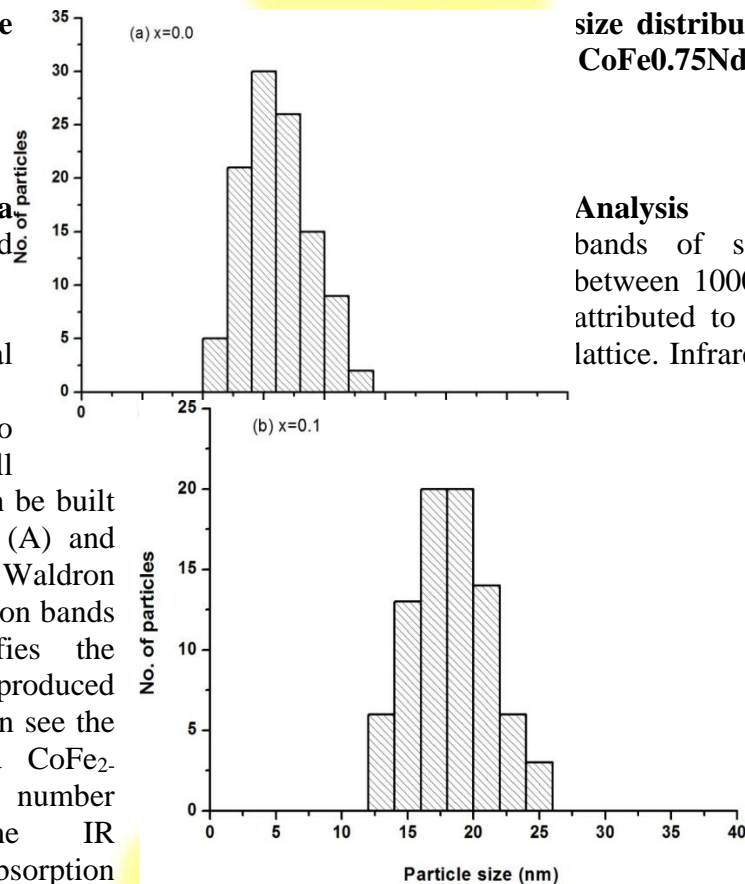**Figure 3(a) The Distribution of Cofe$_2$O$_4$ Nanoparticles**

**Figure 3(b) The size distribution of CoFe0.9Nd0.1O4 nanoparticles**

**Figure 3(c) The** size distribution of **CoFe0.75Nd0.25O4** nanoparticles



**FTIR Spectra Analysis**

The infrared numbers typically the crystal ferrites display two bands. Unit cell cubic spinel can be built tetrahedral site (A) and (B), as stated by Waldron distinct absorption bands spectrum verifies the structure in the produced Figure 4, we can see the of the studied $CoFe_2$- in the wave number $400cm^{-1}$. The IR two major absorption bands of solids, with wave between 1000 and $300cm^{-1}$, are attributed to ionic vibrations in lattice. Infrared spectra of spinel consistently metal-oxygen vibrations of in both the the octahedral site . The presence of in the FTIR creation of spinel materials. In absorption bands $_xNdxO_4$ samples range 900- spectrum exhibits bands. The stretching vibrations of the metal at the tetrahedral site explain the absorption band ( $v_1$) seen in the range $600-550cm^{-1}$. The octahedral-metal stretching mechanism is responsible for the band ( $v_2$) seen between 450 and $400cm^{-1}$. As the neodymium concentration rises, a corresponding shift to the low-frequency side is seen in the values of 1 and 2. The substitution of cations with large ionic radii for those with smaller ones causes a shift in the frequency bands toward lower values. Substitution of $Nd^{3+}$ ions for $Fe^{3+}$ ions at octahedral B sites is responsible for the 2 absorption band shift. Since it is well established that a larger site radius results in a lower fundamental frequency, the center frequency should move downward.When smaller $Fe^{3+}$ ions are swapped out for bigger $Nd^{3+}$ ions at the octahedral site, an expansion of the site radius is possible.

**Figure 4 FTIR spectra of CoFe$_{2-x}$NdxO$_4$ system**

**Analysis of Elements by WD-XRF**

Powder sample stoichiometry was verified through WD-XRF analysis. Table 2 provides the elemental composition of CoFe$_{2-x}$NdxO$_4$ samples at x=0.0, x=0.1, and x=0.25 respectively. The stoichiometry of the samples is as anticipated. The absence of any impurity traces suggests that the samples possessed excellent chemical homogeneity.

**Table 2 Elemental analysis of CoFe$_{2-x}$NdxO$_4$ samples with x=0.0, 0.1 and 0.25**

| Elements present | X=0.0 | | X=0.10 | | X=0.25 | |
|---|---|---|---|---|---|---|
| | Expected (wt.%) | WD-XRF (wt.%) | Expected (wt.%) | WD-XRF (wt.%) | Expected (wt.%) | WD-XRF (wt.%) |
| Co | 25.110 | 25.25 | 24.205 | 24.090 | 22.950 | 22.200 |
| Nd | 0 | 0 | 05.924 | 06.516 | 14.046 | 15.051 |
| Fe | 47.608 | 47.30 | 43.586 | 42.810 | 38.072 | 37.080 |
| O | 27.261 | 27.30 | 26.271 | 26.200 | 24.914 | 24.810 |

**MAGNETIC PROPERTIES**

Utilizing a vibrating sample magnetometer, the magnetic properties of the samples were determined, and magnetic hysteresis loops were generated for each sample. For each sample, magnetic parameters including saturation magnetization (Ms), coercivity (Hc), and remanent ratio (R) were calculated. The magnetic hysteresis loops of the CoFe$_{2-x}$NdxO$_4$ system are illustrated in Figure.5. Within the figure's inset are depicted the loops spanning the range of -1.5kOe to 1.5kOe. Despite applying the maximum field of 20kOe, the magnetization remains non-saturated due to various factors, such as the existence of antiferromagnetic or paramagnetic impurities. As a result, the saturation magnetization of each sample was calculated by extrapolating the inverse of the graph illustrating the relationship between field and magnetization to 1/H=0. Table 3 contains the values for the saturation magnetization Ms, coercivity Hc, and remanent ratio R of each sample. The undoped sample exhibits a Ms value of 52.24emu/g at ambient temperature, which is approximately 35% less than the value reported for bulk cobalt ferrite [4]. The decrease in saturation magnetization relative to the bulk magnetization could potentially be attributed to the canting of spins occurring on the nanoparticle surface, resulting in a reduction in the net magnetization .
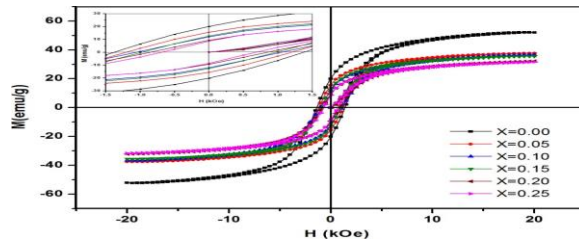
**Figure 5 Room temperature hysteresis curves of CoFe$_{2-x}$NdxO$_4$ system**

As Nd$^{3+}$ contamination increases, the value of saturation magnetization falls from 52.24emu/g to 31.74emu/g. The relationship between the net magnetic moment of ferrites and the distribution of magnetic ions across tetrahedral and octahedral sites is direct. Due to their substantial ionic radii, neodymium ions preferentially adhere to octahedral sites. The ordering of the magnetic moments of rare earth ions can be observed at extremely low temperatures .Rare earth ions' magnetic moments are typically generated by localized 4f electrons. Hence, the impact of Nd$^{3+}$ ions in cobalt ferrite materials appears to be comparable to the replacement of non-magnetic elements in the octahedral Fe sites of the spinel lattice. This substitution results in a reduction of Fe$^{3+}$-Fe$^{3+}$ interactions, thereby leading to a decrease in Ms. Consequently, an increase in neodymium concentration leads to a deterioration in the exchange interaction between octahedral and tetrahedral sites, resulting in a reduction in the magnetization of doped cobalt ferrite. The reduction in magnetization can also be ascribed to the existence of hematite phase, which possesses weak magnetism and is a canted antiferromagnetic at room temperature.

**Table 3 Effect of Nd$^{3+}$ doping on magnetic parameters of CoFe$_{2-x}$NdxO$_4$**

| Nd Content | M$_s$ (emu/g) | M$_r$ (emu/g) | H$_c$ (O$_e$) | R |
|---|---|---|---|---|
| 0.00 | 52.24 | 20.07 | 1379.20 | 0.3842 |
| 0.05 | 37.64 | 15.57 | 961.01 | 0.4137 |
| 0.10 | 36.65 | 12.00 | 863.67 | 0.3274 |
| 0.15 | 35.59 | 12.65 | 852.15 | 0.3554 |
| 0.20 | 32.21 | 09.32 | 803.29 | 0.2894 |
| 0.25 | 31.74 | 08.64 | 686.37 | 0.2722 |

As an indicator of the intensity of the magnetic field necessary to overcome anisotropy and reverse the magnetic moments, the Nd$^{3+}$ substitution has a discernible effect on the coercivity H$_c$. The samples exhibit coercivity values ranging from 1379 to 686Oe, which surpasses the values obtained for cobalt ferrite doped with rare earths that were synthesized using alternative techniques and sintered at 673K.Coercivity is reportedly dependent on magneto-crystallinity, microstrain, size distribution, anisotropy, and the extent of the magnetic domain .Additionally, it is widely recognized that the coercivity in the multidomain regime exhibits an inverse relationship with particle size. An increase in particle size facilitates the movement of domain walls, resulting in a reduction in coercivity. This could potentially account for the decline in coercivity. The observed reduction in Hc value as Nd$^{3+}$ concentration rises may also be attributed to the migration of Co$^{2+}$ ions from octahedral to tetrahedral sites. However, additional research is necessary to validate this. The remanent ratio (R=Mr/Ms) serves as an indicator of the simplicity with which the magnetization reorients itself towards the axis that is closest to it once the magnetic field has been eliminated. The remanent ratio values of the prepared samples fall within the interval of 0.2 to 0.4. The isotropic character of the material is indicated by the low value of R . Consequently, the aforementioned research indicates that

the magnetic characteristics of cobalt ferrite nanoparticles can be modified by manipulating the concentration of neodymium ions.

## ELECTRICAL SPECIFICATIONS

**Resistivity to DC:** The relationship between temperature and DC resistivity for the four samples (x=0.0, 0.05, 0.1, 0.15), as illustrated in Figure 6. It was discovered that the resistivity of the samples increased as the neodymium content rose. The substitution of $Nd^{3+}$ ions for $Fe^{3+}$ ions leads to a reduction in the number of $Fe^{3+}/Fe^{2+}$ ion pairs at the octahedral sites, thereby augmenting the electrical resistivity of the cobalt ferrite that has been doped. Therefore, the rise in resistivity can be ascribed to the reduction in the mobility of charge carriers and the elongation of the B-site hopping distance. The increase in thermal mobility of charge carriers is the cause of the decrease in electrical resistivity with temperature. When the temperature increases, the energy needed to transition an electron between two equivalent lattice sites decreases .The activation energy for hopping exhibits a range of 0.65 eV to 0.74 eV, as determined by the slope of the linear plot of ln ρ versus 1000/T.
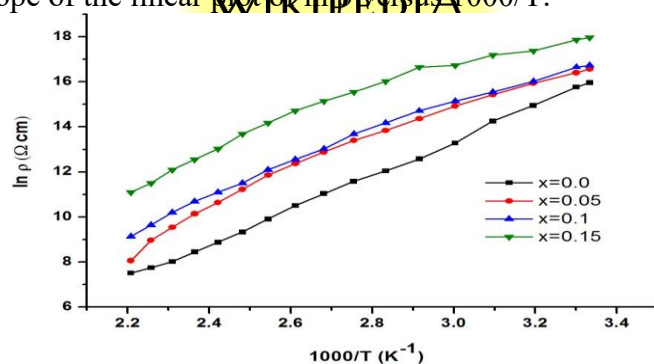


**Figure 6 : Compositional variation of DC resistivity of $CoFe_{2-x}Nd_xO_4$ with inverse temperature**

### Permittivity of Relative Dielectrics

The relationship between frequency and the real part of dielectric permittivity at room temperature is illustrated in Figure 4.
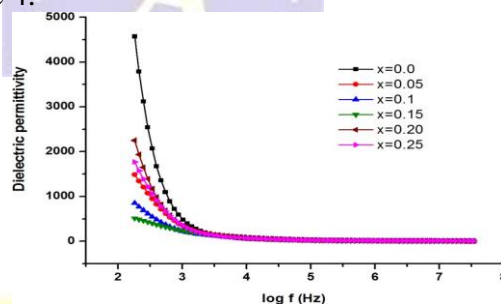


**Figure 7: Dielectric permittivity as a function of log f for $CoFe_{2-x}Nd_xO_4$**

At lower frequencies, the value of the dielectric constant is exceptionally high; as frequency increases, this value swiftly decreases. This is the typical dielectric behavior of spinel ferrites, which numerous researchers have also documented. The correlation between permittivity and frequency can be elucidated through the lens of Koop's theory, which posits that the dielectric structure comprises two layers of an inhomogeneous medium of the Maxwell-Wagner type. As a result of the existence of ferrous and ferric ions, ferrites are dipolar. An external electric field can induce electron hopping between these ions, which can be represented graphically as the rotation of dipoles; this causes orientation polarization. The electronic, ionic, space charge, and dipolar polarizations all contribute to the net polarization of the ferrite material at low frequencies. However, the electron exchange between ferrous and ferric ions ceases to track the alternating field at higher frequencies, causing the contribution of dipolar polarization to the dielectric constant to diminish. Thus, with increasing frequency, the dielectric constant of

the samples decreases. The octahedral site is occupied by neodymium during its incorporation into spinel cobalt ferrite, resulting in a reduction of the $Fe^{3+}$ ion count that governs polarization within the ferrite system. The reduction in magnitude of the hopping rate impedes the conduction mechanism. As a result, the dielectric permittivity of the current system decreases as the $Nd^{3+}$ content rises. Figure 8 illustrates the temperature dependence of dielectric permittivity at specific frequencies for the sample with x=0.1. At each of the chosen frequencies, an increase in temperature results in a corresponding rise in dielectric permittivity. The correlation between the rise in $\varepsilon_r$ and temperature can be attributed to the augmented drift mobility of charge carriers. Additionally, thermal activation increases electron hopping, which results in an increase in hopping frequency. As a consequence, the polarization experiences an upward trend, which subsequently causes the dielectric constant to increase in accordance with the temperature . Ionic, electronic, interfacial, and dipolar polarizations all contribute to the ferrite material's dielectric permittivity. Low frequencies are dominated by dipolar and interfacial contributions, both of which are temperature dependent. This explains why the dielectric constant increases rapidly with temperature when operating at low frequencies. Elevated frequencies are characterized by the predominance of electronic and ionic polarizations, which exhibit negligible temperature dependence .
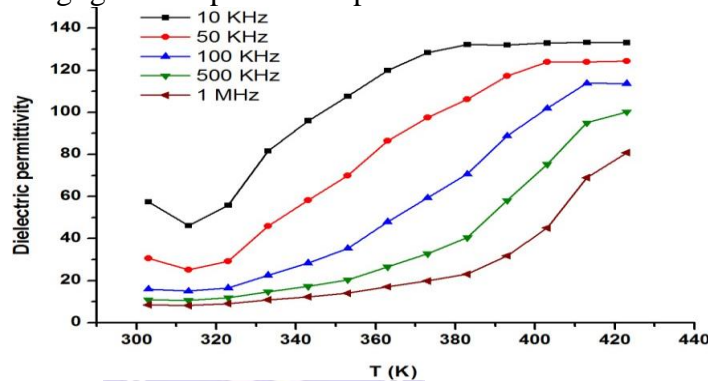


**Figure 8 :Dielectric permittivity as a function of temperature at selected frequencies**
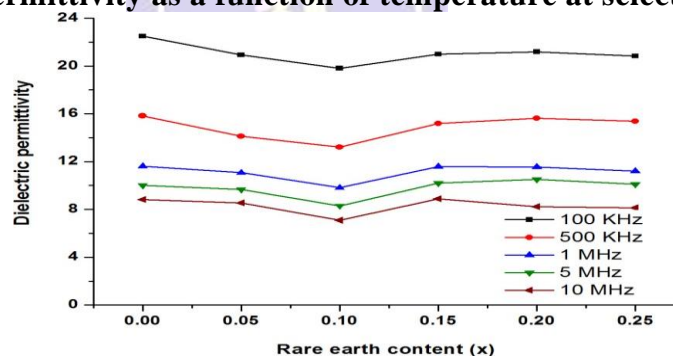


**Figure 9 : Dielectric permittivity as a function of rare earth content at selected frequencies**

The relationship between $Nd^{3+}$ concentration and dielectric permittivity decrease is apparent from Figure 9. At x=0.1, a marginal decline in $\varepsilon_r$ is observed, followed by a marginal ascent. It is well understood that the process by which ferrites undergo dielectric polarization resembles that of electric conduction. When $Nd^{3+}$ ions are used in place of $Fe^{3+}$ ions in the octahedral sites, the rate of electron hopping is reduced, which impedes the conduction mechanism .Thus, the decrease in $\varepsilon_r$ with composition can be explained by the decrease in conductivity with neodymium content.

**Loss of Dielectric:** Dielectric loss exhibits a notable decline during the low frequency range. An eventual state of frequency independence is reached where the rate of decrease diminishes as the frequency rises. Elevated energy expenditure for electron hopping in the low frequency

## RŒTINDEXING
JOURNAL ABSTRACTING AND INDEXING SERVICE

**INTERNATIONAL ADVANCE JOURNAL OF ENGINEERING, SCIENCE AND MANAGEMENT (IAJESM)**
**January-June 2023, Submitted in February 2023, iajesm2014@gmail.com, ISSN -2393-8048**
Multidisciplinary Indexed/Peer Reviewed Journal. SJIF Impact Factor 2023 =6.753

region may account for the observed substantial loss. As the energy necessary for electron hopping is reduced in the high frequency region, dielectric loss also diminishes . The dielectric loss angle diagram of the doped samples exhibits the presence of a peak. The aforementioned peak is identified when the electron hopping frequency between $Fe^{2+}$ and $Fe^{3+}$ is nearly equivalent to the field strength applied externally . The enhanced resistivity and reduction in dielectric constant and losses of these materials make them highly prospective for implementation in low-frequency motors and transformer cores.
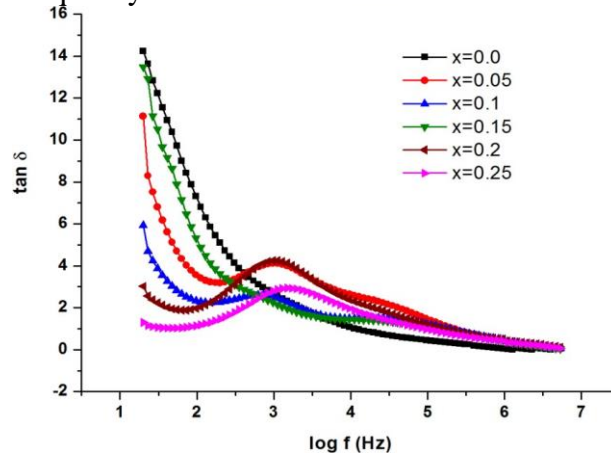


**Figure 10: Variation of dielectric loss tangent with frequency**

**Conductivity of AC**

An illustration of the relationship between AC conductivity and frequency at ambient temperature can be observed in Figure 11. The relationship between frequency and AC conductivity is nearly direct in the majority of disordered solids. Conduction occurs in an ionic lattice as a result of electron hopping between identical elements in various oxidation states. In the case of large polaron hopping, AC conductivity decreases with frequency . Conversely, for small polaron hopping, AC conductivity increases with frequency. Presently, AC conductivity increases with frequency, and at high frequencies, the plots are nearly linear. This suggests that
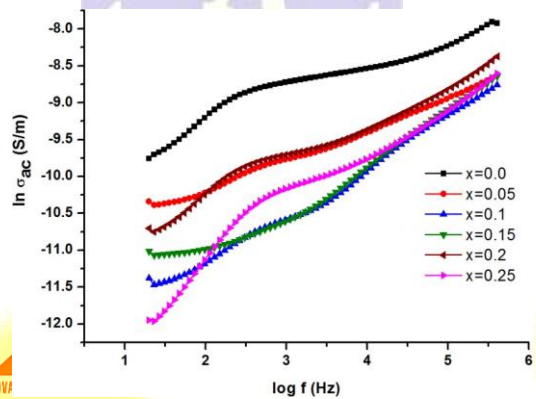


conduction is the result of minor polaron hopping. Small polaron formation may result from oxygen vacancies or defect levels introduced during sintering. The Frequency Dependence of Ac can Be Elucidated Using the Two-Layer Model of Polycrystalline Ferrites by Maxwell and Wagner .

**Figure 11 : AC conductivity ($\sigma_{ac}$) frequency dependence**

Figure 12 illustrates the correlation between absolute temperature and AC conductivity at specific frequencies for the doped sample with x=0.1. At low temperatures, dispersion is observed, whereas at high temperatures, conductivity becomes less temperature dependent. The analogy between the AC conductivity profiles and the real part of the dielectric permittivity

is to be anticipated, given that the square root of conductivity directly influences the dielectric permittivity .
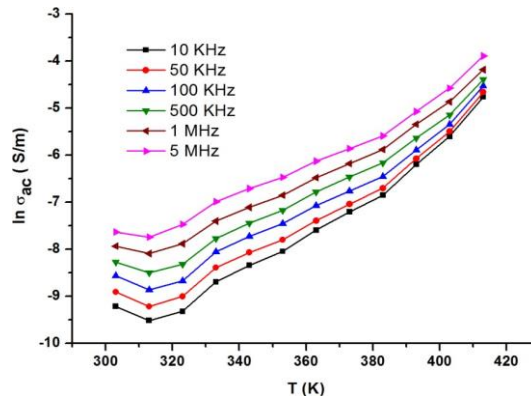


**Figure 12 Relation between AC conductivity and absolute temperature**

As a result of the increase in hopping frequency and mobility caused by a rise in temperature, conductivity increases dramatically. At elevated temperatures, thermal energy is sufficient to induce significant lattice vibrations. This results in the dispersion of charge carriers, which is anticipated to reduce their mobility and consequently reduce the temperature dependence of conductivity. Analogous findings have been documented. The relationship between composition and AC conductivity is illustrated in Figure 13. The reduction in AC conductivity that has been observed can be accounted for by the decrease in hopping rate caused by the replacement of $Fe^{3+}$ ions on the octahedral sites with $Nd^{3+}$ ions. Nevertheless, a marginal rise is observed in the sample containing concentration x=0.2. This increase could potentially be ascribed to the occupancy of the tetrahedral site by the rare earth ion.
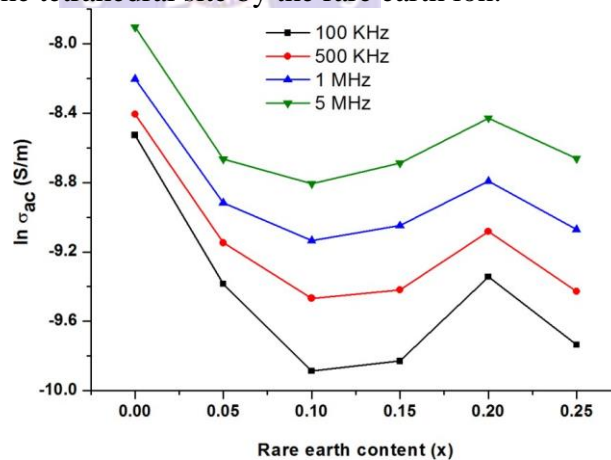


**Figure 13 Variation of AC conductivity ($\sigma_{ac}$ ) with composition (x) at selected frequencies**

**CONCLUSIONS**

Using the sol-gel method, a series of neodymium-doped cobalt ferrites ($CoFe_{2-x}Nd_xO_4$; x=0.0, 0.05, 0.1, 0.15, 0.2, and 0.25 were effectively synthesized. XRD analysis validated the formation of a spinel structure consisting of a single phase. The increase in lattice parameter caused by neodymium doping can be attributed to the greater ionic radius of $Nd^{3+}$ in comparison to $Fe^{3+}$. Neodothium concentration-dependent growth of the crystallite size of cobalt ferrite nanoparticles was observed. The prepared nanoparticles have a spherical morphology, a narrow size distribution, and are faintly agglomerated, as determined by TEM analysis. XRF elemental analysis was utilized to validate the chemical homogeneity of the samples. The presence of absorption bands within the anticipated range in the FTIR spectra provides further support for the spinel properties exhibited by the prepared samples. A reduced frequency shift in the absorption band (2) signifies the substitution of $Fe^{3+}$ ions with $Nd^{3+}$ ions

at the octahedral sites. The observed reduction in saturation magnetization as the neodymium content increased can be attributed to the decline in the net magnetic moment within the octahedral site. Moreover, it is widely recognized that the introduction of rare earth metal ions doped into ferrites reduces the saturation magnetization due to the paramagnetic characteristics and reduced magnetic moment of these ions in comparison to the ferromagnetic $Fe^{3+}$ ions. The correlation between neodymium doping and coercivity in the multidomain regime is elucidated by the particle size dependence of coercivity. The DC electrical resistivity of the doped samples exhibited an initial increase in response to neodymium concentration of x = 0.15, followed by a subsequent decrease as the concentration continued to rise. It can be deduced from the examination of the dielectric properties of the samples doped with neodymium that the introduction of $Nd^{3+}$ ions in lower concentrations reduced the dielectric permittivity and dielectric loss. Moreover, as the frequency of the applied AC field increased, both the dielectric constant and dielectric loss of each sample decreased. This phenomenon can be elucidated through the utilization of the Maxwell-Wagner interfacial polarization and electron hopping mechanisms. Temperature increases the dielectric constant and AC conductivity, which is proportional to the increase in drift mobility, which causes charge carrier hopping frequencies to increase. At high frequencies, the AC conductivity exhibits a linear increase, indicating that the conduction is the result of minor polaron hopping. By carefully selecting the concentration of neodymium ions, it is possible to modify the magnetic and electrical characteristics of cobalt ferrite nanoparticles, thereby rendering them suitable for various technological applications.

## REFERENCES

1. O. Kurni, M. S. Seehra, A. Gupta, A. D. Bristow, "Effect of Neodymium Substitution on the Structural and Magnetic Properties of Cobalt Ferrite Nanoparticles", Journal of Applied Physics, vol. 107, no. 9, 2010, pp. 09D513.

2. S. K. Jain, R. Mathur, R. Gupta, "Effect of neodymium substitution on structural, magnetic and electrical properties of cobalt ferrite nanoparticles", Journal of Magnetism and Magnetic Materials, vol. 321, no. 18, 2009, pp. 2936-2940.

3. D. Varshney, A. Singh, R. J. Singh, "Effect of Neodymium Substitution on Structural, Electrical and Magnetic Properties of Cobalt Ferrite Nanoparticles", Materials Research Bulletin, vol. 50, 2014, pp. 1-6.

4. K. Pradhan, A. V. Rane, R. S. Katiyar, "Effect of Neodymium Substitution on the Structural, Magnetic, and Dielectric Properties of Cobalt Ferrite Nanoparticles", Journal of Applied Physics, vol. 103, no. 7, 2008, pp. 07D522.

5. A. Tadjarodi, M. Akbarzadeh Pasha, S. Z. Mortazavi, "Structural and magnetic properties of cobalt ferrite nanoparticles prepared by a modified sol-gel method and the effect of neodymium substitution", Ceramics International, vol. 40, no. 7, 2014, pp. 10121-10130.

6. S. Giri, D. Goswami, S. Manna, R. Nath, S. Datta, A. Ghosh, "Structural, Magnetic and Electrical Properties of Neodymium Substituted Cobalt Ferrite Nanoparticles", Journal of Nanoscience and Nanotechnology, vol. 14, no. 10, 2014, pp. 7952-7959.

7. B. Raju, M. V. R. Murthy, K. K. Singh, "Effect of Neodymium Substitution on the Structural and Magnetic Properties of Cobalt Ferrite Nanoparticles", International Journal of Engineering and Advanced Technology, vol. 8, no. 6, 2019, pp. 3150-3156.

8. S. Kumar, A. K. Pradhan, S. Das, J. Mathur, A. K. Jha, "Effect of neodymium substitution on structural, magnetic and electrical properties of cobalt ferrite nanoparticles synthesized by citrate gel method", AIP Conference Proceedings, vol. 1512, 2013, pp. 640-641.

9.  S. Pradhan, B. Panda, "Influence of Neodymium Substitution on Structural and Magnetic Properties of Cobalt Ferrite Nanoparticles Synthesized by Sol-Gel Method", Journal of Nanomaterials, vol. 2017, 2017, pp. 8230473.

10. S. Manikandan, M. D. Narayanan, G. L. Murali, "Effect of neodymium substitution on structural and magnetic properties of cobalt ferrite nanoparticles", AIP Conference Proceedings, vol. 1665, 2015, pp. 050046.

11. V. Anil Kumar, M. S. Varalakshmi, "Effect of neodymium substitution on structural, magnetic and dielectric properties of cobalt ferrite nanoparticles", AIP Conference Proceedings, vol. 2224, 2020, pp. 020059.

12. J. Liu, H. Hu, Y. Zhang, Y. Li, "Effect of Neodymium Substitution on the Structural and Magnetic Properties of Cobalt Ferrite Nanoparticles Synthesized by Sol-Gel Method", Materials Science and Engineering: B, vol. 186, 2014, pp. 103-108.